https://doi.org/10.5194/egusphere-2026-3224
Preprint. Discussion started: 22 June 2026

Gravimetrically Measured Water Content of Filter Sampled Fine Particulate Matter at Low Relative Humidity: Insight from the Surface Particulate Matter Network (SPARTAN)

Author list: Christopher R. Oxford[1]*, Haihui Zhu[1,2], Maya Mehrotra[1], Xuan Liu[1,3], Yuxuan Ren[1], Maya Arnott[1], Isaac Abionum Adimula[4], Taiye Benjamin Ajibolataiye[4], Clement Akoshile[4], Omar Amador-Munoz[5], Araya Asfaw[6], Rachel Ying-Wen Chang[7], Sagnik Dey[8,9], Ann M. Dillner[10], David J. Diner[11], Connor J. Flynn[12], Diana Francis[13], Paterne Gahungu[14], Rebecca M. Garland[15,16], Michel Grutter[5], Sina Hasheminassab[11], Fahad Imam[8], Jhoon Kim[17], Kristy Langerman[18], Pei-Chen Lee[19], Puji Lestari[20], Po-Hsiung Lin[21], S. Marcela Loria-Salazar[12], Tesfaye Mamo[22], Olga L. Mayol-Bracero[23], Mogesh Naidoo[15], Narendra Nelli[13], Sang Seo Park[24], Abdus Salam[25], Bighnaraj Sarangi[23], Trailokya Saud[26] , Robyn Schofield[27], Yoav Schechner[28] Sachchida N. Tripathi[29], Emily K. West[12], Eli Windwer[30], Ming-Tsang Wu[31,32], Qiang Zhang[33], Michael Brauer[34], Yinon Rudich[30], Jay R. Turner[1], and Randall V. Martin[1]

[1] Department of Energy, Environmental & Chemical Engineering, Washington University in St. Louis, St. Louis, Missouri 63130, United States

[2] Department of Atmospheric Science, Colorado State University, Fort Collins, Colorado 80521, United States

[3] Scripps Institution of Oceanography, University of California San Diego, San Diego, California 92093, United States

[4] Department of Physics, University of Ilorin, Ilorin, 240003, Nigeria

[5] Instituto de Ciencias de la Atmósfera y Cambio Climático, Universidad Nacional Autónoma de México, Mexico City, 04510, Mexico

[6] Institute of Geophysics and Space Science, Addis Ababa University, Addis Ababa,1176, Ethiopia

[7] Department of Physics and Atmospheric Science, Dalhousie University, Halifax, Nova Scotia B3H 4R2, Canada

[8] Indian Institute of Technology Delhi, Hauz Khas, New Delhi, India 110016

[9] Adjunct Faculty, Department of Health, Management and Policy, Korea University, Seoul, South Korea

[10] Air Quality Research Center, University of California Davis, Davis, CA, USA

[11] Jet Propulsion Laboratory, California Institute of Technology, Pasadena, California, United States

[12] School of Meteorology, University of Oklahoma, Norman, Oklahoma, United States

[13] Environmental and Geophysical Sciences Lab, Earth Science Department, Khalifa University, Abu Dhabi, 127788, United Arab Emirates

[14] Institute of Applied Statistics, University of Burundi, Bujumbura, BP1550, Burundi

[15] Council for Scientific and Industrial Research, Pretoria, 0001, South Africa

https://doi.org/10.5194/egusphere-2026-3224
Preprint. Discussion started: 22 June 2026

[16] Department of Geography, Geo-Informatics and Meteorology, University of Pretoria, Pretoria, 0002, South Africa

[17] Department of Atmospheric Sciences, Yonsei University, Seoul, 03722, Republic of Korea

[18] Department of Geography, Environmental Management and Energy Studies, University of Johannesburg, Johannesburg, 2006, South Africa

[19] Department of Public Health, National Cheng Kung University, Tainan, 701, Taiwan

[20] Faculty of Civil and Environmental Engineering, Bandung Institute of Technology, Bandung, 40132, Indonesia

[21] Department of Atmospheric Sciences, National Taiwan University, Taipei, Taiwan

[22] Department of Physics, Addis Ababa University, Addis Ababa, Ethiopia

[23] Department of Environmental Science, University of Puerto Rico, Puerto Rico, 00931, United States

[24] Department of Urban and Environmental Engineering, Ulsan National Institute of Science and Technology, Ulsan, 44919, Republic of Korea

[25] Department of Chemistry, University of Dhaka, Dhaka, 1000, Bangladesh

[26] National Aerosol Facility, Indian Institute of Technology Kanpur, Kanpur, 208016, India

[27] School of Geography, Earth and Atmospheric Sciences, University of Melbourne, Melbourne, 3010, Australia

[28] Department of Electrical Engineering, Technion Israel Institute of Technology, Haifa, 3200003, Israel

[29] Kotak School of Sustainability, Indian Institute of Technology Kanpur, Kanpur, 208016, India

[30] Department of Earth and Planetary Sciences, Weizmann Institute of Science, Rehovot, 76100, Israel

[31] Department of Family Medicine, Kaohsiung Medical University Hospital, Kaohsiung Medical University, Kaohsiung, 807, Taiwan

[32] PhD Program in Environmental and Occupational Medicine, Kaohsiung Medical University, Kaohsiung, 807, Taiwan

[33] School of Environment, Tsinghua University, Beijing, 100084, China

[34] School of Population and Public Health, University of British Columbia, Vancouver, British Columbia V6T 1Z3, Canada

* Corresponding author Christopher R. Oxford. email: coxford@wustl.edu

Keywords: PTFE filters, hygroscopicity,

https://doi.org/10.5194/egusphere-2026-3224
Preprint. Discussion started: 22 June 2026

Short summary: A high-sensitivity balance, controlled temperature and relative humidity chamber, and filter samples collected around the world were used to develop a mass as a function of relative humidity relationship. We subsequently measured the chemical composition of these same samples. A relationship between the chemical composition and water mass was created and used to calculate aerosol water content showing how composition and water content varies worldwide.

Abstract

Accurate measurements of the composition of fine particulate matter ($PM_{2.5}$) are important for understanding its sources and health impacts. Water, a portion of $PM_{2.5}$ mass, is difficult to measure. We describe developments to the Surface PARTiculate mAtter Network (SPARTAN) to better characterize the chemical composition of $PM_{2.5}$ on polytetrafluoroethylene filters. A robotic weighing facility is used to estimate water content of $PM_{2.5}$ sampled at three sites (Fajardo, Puerto Rico; Bujumbura, Burundi; Abu Dhabi, United Arab Emirates), and the chemical composition is used to attribute water content to three hygroscopic categories: high growth (sodium chloride), medium growth (ammonium-nitrate-sulfate-potassium), and low growth (organics). The growth rates are tested using two additional sites (Beijing, China; Halifax, Canada). The water content at 35% relative humidity (RH) is estimated to be 16.5% (11.6%-26.5%, 95% confidence) for the high growth category, 3.9% (3.0%-4.2%, 95% confidence) for medium growth, and 1.0% (0.6-1.3%, 95% confidence) for low growth. We calculate the average water content at 35% RH for 2442 filters from 24 globally distributed sites from December 2019 to September 2024 to be 2.06% (0.85%-5.47%, range), where 58% of the aerosol water is associated with the medium growth category (22% low growth, 19% high growth).

1. Introduction

Exposure to fine particulate matter with an aerodynamic diameter less than 2.5 μm ($PM_{2.5}$) is associated with increased mortality (Dockery et al., 1993; Pope et al., 1995) and morbidity (Pope et al., 2004; Brook et al., 2010; Abbey et al., 1998; Abbey et al., 1999). Filter-based measurements of PM are widely utilized for epidemiological studies (Kazemiparkouhi et al., 2022; Wolf et al., 2021), for air quality characterization by regulatory networks (Spengler and Thurston, 1983; Lipfert et al., 1988), to evaluate air quality models (Van Donkelaar et al., 2010; Van Donkelaar et al., 2024), and as a reference for other $PM_{2.5}$ measurement techniques (Noble

https://doi.org/10.5194/egusphere-2026-3224
Preprint. Discussion started: 22 June 2026

et al., 2001). Filter samples of $PM_{2.5}$ and PM_{10} (particulate matter with an aerodynamic diameter less than 10 μm) include the chemical components of mineral dust, black carbon, organic matter, water-soluble ionic species, transition metals, and water (Chow et al., 2015). Methods to measure ionic components (Chow and Watson, 1999), trace elements (Watson et al., 1999), black carbon (White et al., 2016; Chow et al., 1993a), and organic matter (Daellenbach et al., 2016; Ruthenburg et al., 2014; Surratt et al., 2008) are relatively well developed. Measurements of water mass, however, remain absent from filter-based $PM_{2.5}$ measurements.

Water mass on filters depends on both the relative humidity (RH) of the surrounding gas and the composition of the deposited mass. Ionic components, metals, elemental carbon, and organic matter have different affinities for water mass (Mcmurry et al., 1996), and fractional differences in these components alter that total water mass. Additionally, standard protocols to measure $PM_{2.5}$ mass on polytetrafluoroethylene (PTFE) filters vary, with the US EPA using 30-40% RH (Register, 2020), Canada using 35-45% (Dabek-Zlotorzynska et al., 2011), and Europe using 45-50% (Standardization, 2023). Air quality models used for $PM_{2.5}$ prediction and to relate satellite observations of aerosol optical depth with ground-level $PM_{2.5}$ require information on the water content of $PM_{2.5}$ to reconcile calculated $PM_{2.5}$ concentration with observations (Van Donkelaar et al., 2010; Van Donkelaar et al., 2024). Knowledge of the relationship of water content on $PM_{2.5}$ filters as a function of RH and composition is needed to rigorously evaluate air quality models and understand differences across monitoring networks.

Most measurements of water mass in $PM_{2.5}$ filter samples have either applied destructive techniques prohibiting further composition measurements, had weak statistical resolution, required additional instrumentation, or required assumptions about the particle properties. Karl Fisher titration quantifies water mass through a sulfur dioxide-iodide redox reaction (Fischer, 1935). Canepari et al. (2013); (Canepari et al., 2017) applied this method to measure water mass on filters at 50% RH from Rome (3-4%), Ferrara (>10%), Tel Aviv (>10%), Cassana (10-33%), and the Po Valley (2-11%); however, the required heating process irreversibly destroyed all samples. Mikhailov et al. (2013) tried differential katharometry to estimate water in $PM_{2.5}$ samples from the Amazonian Aerosol Characterization Experiment (AMAZE) and from a boreal forest near St. Petersburg, but the method lacked mass resolution at low RH (Tang et al., 2019a). Rees et al. (2004) used the integrated response from a Tandem Differential Mobility Analyzer to estimate water content of aerosols at 35% RH in Pittsburg, finding that water mass fraction was 16% in summer and near 0% in winter; this method required assumptions about both particle shape and density as well as the deployment of a real

https://doi.org/10.5194/egusphere-2026-3224
Preprint. Discussion started: 22 June 2026

time instrument. Speer et al. (2003) used a beta attenuation monitor to estimate the water content of $PM_{2.5}$ sampled in North Carolina, finding a water mass fraction of less than 10% at 35% RH. Mcinnes et al. (1996) used gravimetric mass on several marine samples, finding that coastal samples at Cheeka Peak increased 9% by mass when RH increased from 9% to 35%, and samples from an ocean cruise increased 29% by mass when RH increased from 19% to 47%; unlike some of the methods above, gravimetric weighing did not harm the sample, allowing further compositional analysis.

The Surface PARTiculate mAtter Network (SPARTAN) is a globally distributed network of $PM_{2.5}$ and PM_{10} samplers (Snider et al., 2016). In 2019, SPARTAN relocated its laboratory to Washington University in St. Louis and upgraded its instrumentation with an environmentally controlled robotic weighing facility, a dedicated X-ray fluorescence instrument (Liu et al., 2024), and two dedicated ion chromatography instruments. In this study, we relate water content of deposited aerosol mass using the robotic weighing facility to the chemical constituents measured by the laboratory instruments. We use samples from Bujumbura, Burundi; Fajardo, Puerto Rico; and Abu Dhabi, United Arab Emirates to build this relationship, and samples from Beijing, China and Halifax, Canada to evaluate the relationship. We then use the developed relationship to predict water content for the network.

2. Materials and Methods

2.1. SPARTAN sampling operations

SPARTAN measures the mass concentration and chemical composition of ambient $PM_{2.5}$ and PM_{10} across globally-distributed sites. Chemical composition measurements include black carbon (BC) (Ren et al., 2025), trace elements (Liu et al., 2022; Liu et al., 2024; Mcneill et al., 2020), water-soluble ions (Weagle et al., 2018; Snider et al., 2016), and organic carbon (OC) (Dillner and Takahama, 2015). Site locations prioritize under-sampled, high population density locations for public health relevance (Snider et al., 2015; Snider et al., 2016). Sampling stations are positioned on rooftops away from primary aerosol sources to obtain background aerosol samples, and where possible, are co-located with Aerosol Robotic Network (AERONET) sun photometers (Holben et al., 1998) that measure aerosol optical depth (AOD). Table S1 contains the geo-locations and host institutes of the 24 sites in this study.

An Air Photon SS5 sampling station collected aerosols at each of the 24 sites. Site operators installed each filter cartridge, which contained 8 filters — 7 sample filters plus traveling field blank. The sampling stations operated at two independent flow rates, 5 liters per

https://doi.org/10.5194/egusphere-2026-3224
Preprint. Discussion started: 22 June 2026

minute (LPM) and 1.5 LPM, which, when combined with the Mesa Labs SCC1.829 cyclone, enabled the aerodynamic cut diameters (d_{p50}) to be 2.5 µm and 10 µm, respectively. The penetrating aerosol was deposited on a Measurement Technology Laboratories PT25DMCAN-PF03A 25 mm PTFE filter. See Supplemental Text S1 for a description of PTFE filter acceptance requirements prior to use. After filtration of the aerosol, the clean air passed through the sampling station mass flow meter. The station recorded the flow rate in Standard Liters Per Minute (SLPM), pressure drop in kPa, and temperature in °C every 15 seconds, even when the vacuum pump was inactive. If power loss occurred during sampling, the station recorded the date and time of power loss and power recovery.

Sampling protocols were site specific; Table S2 documents the sampling duration and protocol used at each site. The goal of each protocol was to deposit 100 – 200 µg of aerosol on each PTFE filter at the selected flow rate by changing sampling duration. Sampling duration varied from 12 – 48 hours per filter depending upon the expected aerosol mass concentration at the site. Sites associated with the National Aeronautics and Space Administration (NASA)-Italian Space Agency (ASI) Multi-Angle Imager for Aerosols (MAIA) satellite mission (Diner et al., 2018) sampled one 24-hour $PM_{2.5}$ filter every 3 days (MAIA protocol). Other SPARTAN sites sampled one $PM_{2.5}$ filter every 9 days (SPARTAN protocol) with the sampling hours evenly distributed throughout the sampling period. An example 24-hour SPARTAN protocol is shown in Supplemental Fig. S1.

Once sampling completed, the site operator measured post sampling flow rates using an Omega FL-2040 flow meter and packed the cartridge for shipment. All samples were shipped in sealed containers when returned to the central laboratory at Washington University. Once at the laboratory, the cartridge was disassembled inside an Air Clean 600 (HEPA filtered) workstation, and filters were placed into individual Petri dishes. A group photograph was taken of all 8 filters after disassembly and archived. The Petri dishes were then placed inside an environmental chamber set to 21.5 °C and 35% RH to await weighing.

2.2. SPARTAN laboratory operations

A Measurement Technology Laboratories (MTL) AH500 system weighed the PTFE filters both before and after sampling. The system resides inside an environmental chamber that is also operated at 21.5 °C and 35% RH for an additional tier of environmental control. The balance inside the AH500 system is Mettler-Toledo XPR6UD5 with a resolution of 0.5 µg. To weigh a group of filters, we recorded the date and time each filter entered the AH500

https://doi.org/10.5194/egusphere-2026-3224
Preprint. Discussion started: 22 June 2026

environment. The group of filters then equilibrated inside the AH500 system for 24 hours. The system then performed a quality control procedure consisting of a 3-point calibration of the balance, measuring 3 standard masses (100 mg, 200 mg, and 400 mg National Institute of Standards and Technology (NIST) traceable standard weights), and measuring 3 lot-specific lab blank filters. Each sample filter was then weighed three times, and an average weight, standard deviation, system temperature, and system RH were recorded. Subsequently, the quality control procedure was repeated to ensure system stability throughout the weighing routine. All filters were removed within 48 hours of weighing. We recorded the time and date the filters were removed from the AH500 system and returned to the Petri dishes. Repeated measures of lab blank filters show a precision of 0.5%.

The Petri dishes containing filters were then packaged in sealed containers and shipped to the University of California Davis (UC Davis) for measurement with Hybrid Integrating Plate Sphere (HIPS) (White et al., 2016), as recently summarized (Ren et al., 2025) and Fourier Transform Infrared Spectroscopy (FT-IR) (Debus et al., 2022). HIPS measures the integrated transmittance through and reflectance from a sampled filter (filter + deposit) illuminated by a He-Ne laser (633 μm). This transmittance and reflectance were then converted to a filter absorption measurement (τ_{abs}). Absorption was related to the mass of equivalent BC using a Mass Absorbance Cross-section (MAC) of 10 m^2/g (White et al., 2016). This MAC value empirically relates the absorbance on PTFE filters to the mass of Elemental Carbon (EC) measured using the Thermal Optical Reflectance (TOR) method (Chow et al., 1993b). Fourier Transfer Infrared spectroscopy measurements (Debus et al., 2022; Dillner and Takahama, 2015; Reggente et al., 2016) measurements of organic carbon were made using a Bruker Tensor 2 mid-IR instrument (Bruker Optics, Billerica, MA). The FT-IR spectra were calibrated to TOR OC measurements using IMPROVE spectra and co-located TOR OC data as described in Supplemental Text S2.

After return to the central laboratory at Washington University, all filters were measured using a Malvern PANalytical Epsilon 4 X-Ray Fluorescence (XRF) instrument as described in Liu et al. (2024). This measurement provided masses of individual elements of sodium, aluminum, silicon, sulfur, chlorine, potassium, calcium, titanium, vanadium, iron, zinc, cesium, lead, arsenic, cobalt, chromium, copper, magnesium, manganese, nickel, antimony, rubidium, strontium, cadmium, selenium, and tin. Annual calibrations used a total of 62 standards from Micromatter (Surrey, Canada), NIST, and UC Davis, with the latter of particular value to represent filter material and mass loadings of common ambient $PM_{2.5}$ samples (Yatkin et al., 2018). Monthly calibration checks used UC Davis and NIST standards with representative

https://doi.org/10.5194/egusphere-2026-3224
Preprint. Discussion started: 22 June 2026

SPARTAN samples to confirm existing calibration produces measurements within expected error, and measurement of each cartridge included a lab blank filter, which measured within expected error (Liu et al., 2024).

After XRF, each filter, including the field blank, was individually photographed. The lid of the Petri dish was temporarily removed, and the filter and Petri dish bottom were placed on a background template. Light (5000 K) from strips of Light Emitting Diodes illuminated the template, Petri dish bottom, and filter. A photograph of the filter, Petri dish, and template was taken using a digital Single Lens Reflex (SLR) camera. The resulting photograph was used to provide an additional exploratory estimate of the effective BC (Jeronimo et al., 2020), but all BC data in this study used HIPS. Additionally, this photograph provides a visual record of all filter samples (e.g., Supplemental Fig. S2). After photography, measurements using UV-Visible spectrophotometer (UV-Vis) were conducted for additional information on spectrally resolved absorption (Pandey et al., 2019; Zhong and Jang, 2011) as described in Supplemental Text S3.

After UV-Vis, the filters underwent a water-based extraction. Each filter was placed, aerosol side up, into a 20 ml scintillation vial. The filter was covered with 0.2 ml of High Performance Liquid Chromatography (HPLC) grade methanol (Sigma-Aldrich 646377) and then covered with 5.8 ml of 18 MΩ deionized water. The vial was sealed with a sheet of aluminum foil, a plastic cap, and then sonicated for 30 minutes. Sonication destroyed the filter, and the aerosol was dissolved or suspended in the extractant. The vials were then removed from the sonicator, and the extractant solution was withdrawn by glass syringe. The solution was filtered through a polypropylene syringe filter with a pore size of 0.2 μm. The particle-free extractant was placed in an opaque Nalgene sample vial and stored at 2 °C to await Ion Chromatography analysis. All vials, syringes, and syringe filters were rigorously cleaned as described in Supplemental Text S4.

Two Dionex Integrion ion chromatography systems, one dedicated to anions and one to cations, analyzed the extractant. The cation system used a methane sulfonic acid eluent generation system with a Dionex CS12A column and CG12A guard column. The anion system used either a potassium hydroxide eluent generation system with a Dionex AS18 column and AG18 guard column or used a 2.7 mM sodium carbonate–0.3 mM sodium bicarbonate eluent with a Dionex AS12A column and AG12A guard column. The measured cations included lithium, sodium, ammonium, potassium, magnesium, and calcium; and the measured anions include fluoride, chloride, nitrite, bromide, sulfate, nitrate, and phosphate. The lab blank was used for blank subtraction, which removes solvent peaks. For both systems, calibrations were performed

https://doi.org/10.5194/egusphere-2026-3224
Preprint. Discussion started: 22 June 2026

at the beginning of every measurement procedure, and the calibration standards were made bi-weekly from NIST traceable stock solutions (cation–Dionex 056933; anion–Dionex 046070). Calibration correlations were flagged if they did not exceed 0.995. Water and quality check solutions were dispersed throughout the measurement run to confirm stability throughout. The sample was flagged if (a) the water samples measured more than 10 times method detection limit of any of the 13 measured species or (b) if the quality check solutions deviated more than 10% of mixed concentration.

2.3. SPARTAN mass reconstruction

Table 1 summarizes the mass reconstruction formulas to determine PM mass concentrations, chemical composition, and the associated mass. A global mineral dust equation was used to infer dust mass from measured elements (Liu et al., 2022). Remaining trace elements were treated as oxidized (Liu et al., 2024) and summed into a single category called Trace Element Oxides (TEO). Residual matter was calculated by subtracting from the gravimetric mass all other measured components (including water described below). This residual matter was treated as organic as confirmed by the correlation ($R = 0.89$, $n = 2442$, $p < 0.004$) between FT-IR organic carbon (OC) and the residual. We adopt the residual as the measure of organic matter below to implicitly account for both OC and associated oxygen, hydrogen, and other elements in organic compounds to ensure mass closure.

Table 1. Summary of measurements, equipment, and methods.

Measurement/ component (symbol) [unit]	Method	Equipment	Calculation method	Notes:
Volume of sampled air (V_a) [m^3]	Station recorded uptime/ rotameter volumetric flow rate	AirPhoton SS5 sampling station/ Omega FL2040	$Q_{avg} * time$	
Mass of deposited aerosol (M_{net}) [μg]	Gravimetric balance with environmental control	MTL AH500 with Metler Toledo XPR6UD5 microbalance	M_{post} - M_{pre}	T_{sp}=21.5 C RH_{sp}=35% Environmental set point adjustable
$PM_{2.5}$ or PM_{10} concentration [μg/m^3]	Deposited mass per sampled volume	Mesa Labs SCC 1.829 cyclone	M_{net}/V_a	5 LPM flow rate for $PM_{2.5}$. 1.5 LPM flow rate for PM_{10}
Effective Black Carbon (EBC) [μg]	Filter transmittance and reflectance	Hybrid Integrated Plate Sphere	$A_{cs} * \tau_{abs} \ / \ \sigma$	λ = 633 nm (White et al., 2016) (Ren et al., 2025)

https://doi.org/10.5194/egusphere-2026-3224
Preprint. Discussion started: 22 June 2026

Dust [μg]	Energy Dispersive X-ray Fluorescence	Malvern PANalytical Epsilon 4	$[1.89Al * (1+MAL) + 2.4Si + 1.40Ca + 1.36Fe + 1.67Ti] * CF$	MAL=mineral-to-aluminum ratio. CF is a correction factor. These values vary by region. (Liu et al., 2022)
Trace Element Oxides (TEO) [μg]	Energy Dispersive X-ray Fluorescence	Malvern PANalytical Epsilon 4	$1.79V + 1.69Cr + 1.63Mn + 1.34Co + 1.27Ni + 1.25Cu + 1.24Zn + 1.43As + 1.41Se + 1.09Rb + 1.18Sr + 1.14Cd + 1.20Sn + 1.26Sb + 1.20Ce + 1.12Pb$	(Liu et al., 2024)
Water soluble cations–Sodium, Ammonium, Potassium [μg]	Cation Ion Chromatography	Thermo Scientific Integrion with Dionex CS-12A column	$[Na^+]*V_{ext}$ $[NH_4^+]* V_{ext}$ $[K^+]* V_{ext}$	Eluent is methane sulfonic acid.
Water soluble anions–Sulfate, Nitrate, Chloride [μg]	Anion Ion Chromatography	Thermo Scientific Integrion with AS-12A column or AS-18 column	$[SO_4^{-2}]*V_{ext}$ $[NO_3^-]*V_{ext}$ $[Cl^-]*V_{ext}$	The columns, either AS-12A or AS-18, used Na_2CO_3/$NaHCO_3$ or KOH eluent respectively
Residual (R) [μg]	Mass balance		M_{net}-EBC-$Dust$-TEO-Na^+-NH_4^+-K^+-SO_4^{-2}-NO_3^--Cl−H_2O	Treated as organic based on high correlation with OC

Q_{avg} is the average of the beginning and ending sampling flow rates. Time is the duration of sampling recorded by the sampler. M_{pre} is the mass of a PTFE filter before sampling. M_{post} is the mass of a sampled PTFE filter after sampling. A_{cs} is the deposition area of the PTFE filter. σ is the absorption coefficient (10 m^2/g). The volume of the water/methanol extract (V_{ext}) is 6 ml. τ_{abs} is the absorption optical depth.

2.4. Determination of water mass in $PM_{2.5}$ filters

We used the MTL system which includes a controlled RH chamber and the Mettler-Toledo XPR6UD5 balance to repeatedly weigh filters at multiple RHs. Table 2 shows the sampling dates, sampling protocol, and aggregate mass of the $PM_{2.5}$ samples used in the gravimetric mass versus RH (hygroscopicity) experiment. In this work, we aggregate the net filter masses to reduce noise associated with the low aerosol mass on individual filters. Most sites used the SPARTAN 24-hour sampling protocol (Fig. S1). The Halifax site sampled continuously between the listed dates using two co-located stations. All samples went through the analysis procedures described in Sect. 2.2 until the extraction step. Before extraction, the gravimetric mass measurements as a function of RH were performed as documented below. After the gravimetric mass measurements, the filters were extracted as documented in Sect. 2.2.

https://doi.org/10.5194/egusphere-2026-3224
Preprint. Discussion started: 22 June 2026

Table 2. Samples used in the experiments.

Site City	Description	Sample start	Sample end	N[a]	Aggregate[b] $PM_{2.5}$ mass (µg)	Sampling Protocol (hours)
Abu Dhabi	med. growth	3/20/2024	7/21/2024	12	3399	SPARTAN (24)
Beijing	test	2/21/2022	4/10/2022	6	1187	SPARTAN (24)
Bujumbura	low growth	1/27/2023	6/26/2023	12	2261	SPARTAN (24)
Fajardo	high growth	11/5/2022	3/21/2023	12	342	SPARTAN (24)
Halifax	test	8/26/2022	9/9/2022	12	655	Continuous (48)

[a] N is the number of $PM_{2.5}$ sample filters. [b] The aggregate $PM_{2.5}$ mass is the sum of the mass of deposited aerosol (M_{net}) on all filters at 35% RH.

Before describing the weighing measurements, we first define two weighing terms. The weighing of all filters from a site is called a weighing subgroup. Each weighing subgroup is reported as the aggregate net mass of all filters from the site as shown by a blue x on Figure 1. Table 3 shows the number of times all filters from a given site were reweighed (weighing subgroups per weighing group) at a given RH setpoint, and this set of weighing subgroups is called a weighing group. Weighing subgroups within a given weighing group lie temporally close to one another as shown in Fig. 1.

Each filter from a site was repeatedly weighed 3 or 5 times by the AH500 gravimetric system (Sect. 2.2), and from these repeated weighings, we calculated the average filter mass. The aggregate net mass is the sum of all average net masses from the weighing subgroup.

The number of repeat measurements increased during the study to reduce variance, thus samples using 3 repeat mass measurements had larger variations in average net mass (and aggregate net mass) than samples using 5 repeat measurements. We use the three sites with 5 repeat measurements to develop the relationship and the remaining two sites for testing.

The procedure for each weighing group began with setting the RH in the weighing system and waiting for it to reach the desired RH. Once at setpoint, the filters equilibrated for at least 24 hours before weighing all weighing subgroups. For each weighing subgroup, the system calibrated the balance, weighed the references weights, and performed the subgroup weighing. The group weighing was completed when the determined number of subgroup re-weighings, either 7 or 8, finished. For consistency, the equilibration period was used even when the relative humidity was kept constant as in multiple group weighings at 35% RH for Abu Dhabi samples (see Fig. 1 right panel).

https://doi.org/10.5194/egusphere-2026-3224
Preprint. Discussion started: 22 June 2026

Table 3. The settings and filters used in the experiments.

	N[a]	Repeat measurements per sample	Weighing subgroups per weighing group	Buoyancy correction[b]	Relative humidity setpoints	Evaporation method[c]	Total measurements per weighing group
Beijing	6	3	7 (1st) 8 (all others)	Partial	35-50%	Bridged	126 144
Halifax	12	3	8	Partial	35-55%	Bridged	288
Bujumbura	12	5	8	Full	35-55%	Individual	480
Fajardo	12	5	8	Partial	35-55%	Individual	480
Abu Dhabi	12	5	8	Full	20-55%	Individual	480

[a] N is the number of $PM_{2.5}$ samples measured. [b] Partial buoyancy correction uses atmospheric pressure at Lambert International Airport while Full buoyancy correction uses the measured atmospheric pressure at time of mass measurement. [c] The bridged evaporation method is shown in Fig. 1 left panel, and the Individual evaporation method is shown in Fig. 1 right panel.

We began each site's hygroscopicity experiment at an RH setpoint of either 20% or 35% relative humidity then increased (ascending) to a maximum setpoint of either 50% or 55% and then decreased (descending) the relative humidity to the original starting setpoint. Any error introduced by balance calibration impacts the weighing subgroup aggregate net mass while any deviation from the relative humidity setpoint impacts the entire weighing group. For the high, low, and medium growth samples, there were a total of 480 measurements in each weighing group. Each site's experiment (all weighing groups) was performed without removing filters from the AH500 environment.

The changes in net filter mass were quite small and often within the influence of buoyancy, which is driven by changes in system temperature, pressure, and RH. Temperature and RH were measured by the AH500 system during each weighing and every minute throughout the study. A Vaisala PTB330 barometer was added to the system partway through the study, enabling full buoyancy correction. Prior to this addition, system pressure was estimated as the atmospheric pressure recorded at Lambert International Airport, 11 km away. Calculations using atmospheric pressure from the airport were called partially corrected as they were corrected for atmospheric pressure but not for the influence of other factors like the ambient conditioning unit. In all cases, to calculate buoyancy, the density of air is calculated using the equations from Devres (1994).

The total AH500 measurement duration (weeks) for each sample was long enough to require estimation of aerosol evaporation in conjunction with hygroscopic measurements. Figure 1 shows the two methods used to estimate evaporation of the aerosol sample: a bridging method suitable for shorter durations and an individual method that achieves independence of

https://doi.org/10.5194/egusphere-2026-3224
Preprint. Discussion started: 22 June 2026

ascending and descending sections but requires a longer analysis period. The Beijing and Halifax samples used the bridging technique shown in the left panel. A linear evaporation line was drawn between the initial 35% RH weighing group and the final two 35% RH weighing groups. The difference between any weighing subgroup and the evaporation line represented the additional water mass resulting from an increase in RH. The filters from Abu Dhabi, Bujumbura, and Fajardo used separate evaporation lines: one for the ascending and one for the descending RH sections of the experiment as shown in the right panel of Fig. 1. Five or six 35% RH weighing groups are used to establish aerosol evaporation in both the ascending and descending branches. The fifth (temporally) 35% RH weighing group of the ascending evaporation line is used in conjunction with the 45% and 55% weighing groups to establish the ascending RH-gravimetric relationship in Figs. 2 and 3 below. The descending RH-gravimetric relationship used the first (temporally) of the last 6 35% RH weighing groups in Figs. 2 and 3 below. The Abu Dhabi samples were also weighed at 20% RH; thus, the difference between the evaporation line and the 20% weighing subgroups represented the water mass lost at the lower RH. We use the three sites with the more robust individual method to develop the water mass relationships, and the remaining two sites with bridging techniques for testing.

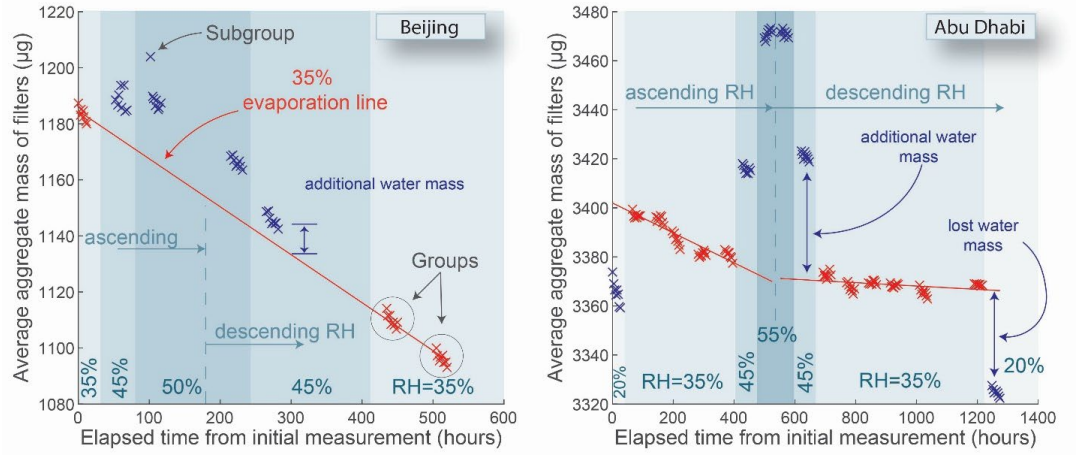

Figure 1. The RH-gravimetric methods used to estimate the evaporation of the aerosol. The left panel uses a bridging technique to determine the evaporation rate of the aerosol. The red evaporation line connects measurements at 35% RH (red x's). The change in water mass due to increases in RH is equivalent to the difference between the aggregate mass (blue x's) and the evaporation line. The right panel uses two individual evaporation lines, one for ascending RH and one for descending RH. In both panels, the shading represents the different RH's in the experiments.

In both methods, we assumed that evaporation could be modeled linearly over the experimental period. This linear assumption is justified by the short duration of the experiment

https://doi.org/10.5194/egusphere-2026-3224
Preprint. Discussion started: 22 June 2026

compared to the total time required to evaporate all particles (Supplemental Text S5 contains an explanation and a visual representation).

Activity models were fit to the discrete RH-gravimetric data. Three activity models were used to extrapolate each hygroscopicity experiment (ascending or descending): Henry's law (Tester and Modell, 1997) (Eq. 1), kappa-hygroscopicity (Mikhailov et al., 2013) (Eq. 2), and the Wilson equation (Wilson, 1964) (Eq 3).

$$RH = x_w H_w \quad (1)$$

$$RH = \frac{M_w}{M_w + \kappa M_a} \quad (2)$$

$$RH = x_w exp\left\{-ln[x_w + x_a\Delta_{wa}] + x_a\left[\frac{\Delta_{wa}}{x_w + x_a\Delta_{wa}} - \frac{\Delta_{aw}}{x_w\Delta_{aw} + x_a}\right]\right\} \quad (3)$$

x_w is the mass fraction of water, H_w is the Henry's law coefficient, M_w is the mass of water, κ is the hygroscopicity coefficient, M_a is the mass of aerosol, x_a is the mass fraction of aerosol, Δ_{wa} is the first Wilson constant, and Δ_{aw} is the second Wilson constant. The mass fraction of water is $M_w/(M_w+M_a)$. To fit the three models to the discrete data, we minimized the square difference in aggregate $PM_{2.5}$ mass between the model and data. The activity models were then extrapolated to 0% RH to determine dry mass and percent water at each RH.

We apportioned the water mass response to three categories: high growth, medium growth, and one low growth. This methodology is conceptually similar to the reproduction of Cloud Condensation Nucleus activation data using multiple growth categories (Hong et al., 2014; Martin et al., 2011). In the high growth category, we sum the measured mass of the sodium ion and the chloride ion since sodium chloride is a high growth atmospheric salt. In the medium growth category, we sum the masses of ammonium, nitrate, sulfate, and potassium ions since ammonium nitrate, ammonium sulfate, potassium nitrate, and potassium sulfate have mass growth factors that are half of sodium chloride (Tang, 1997). The low growth category is the residual, which is treated as organic.

The three other components from the chemical speciation measurements (black carbon, dust, and trace element oxides) are treated as hydrophobic (no growth). Although there are instances where both black carbon and dust adsorb water (Su et al., 2024; Tang et al., 2019b), the components responsible for water adsorption are the inorganic ions (e.g., sulfate, nitrate, sodium, ammonium, chloride) and organic constituents within the black carbon and dust. Black carbon or dust without additional ions is generally hydrophobic (Weingartner et al., 1997; Chen

https://doi.org/10.5194/egusphere-2026-3224
Preprint. Discussion started: 22 June 2026

et al., 2020). Trace element oxides are also treated as hydrophobic (Babela and Lamorena, 2020).

To attribute water to these categories, we estimated the water fraction of sampled atmospheric aerosol from three proxy sites. Each of the three sites is dominated by one of the categories above. The Fajardo site located on the Northeast coast of Puerto Rico has the largest sodium chloride fraction in SPARTAN and is the high growth proxy. The Abu Dhabi site located in Masdar city, United Arab Emirates has the largest sulfate fraction in SPARTAN and is the medium growth proxy. The Bujumbura site located in eastern Bujumbura, Burundi has the largest residual in SPARTAN and is the low growth proxy. These proxies also contain mass from other categories. Thus the simultaneous solution attributing water to the categories considers the entire aerosol mixture. The two sites used to test the effectiveness of the resulting relationship have different characteristics. The Beijing site located at Tsinghua University has the largest nitrate fraction in SPARTAN. The Halifax site located at Dalhousie University has the smallest no-growth fraction of all the samples.

3. Results and Discussion

3.1. Gravimetric response of proxy site sample

Figure 2 displays the $PM_{2.5}$ mass as a function of RH for each proxy sample after correcting for evaporation and bouyancy as described in Sect. 2.3. The original data for Abu Dhabi is found in Fig. 1 while Fajardo is found in Supplemental Fig. S4 and Bujumbura in Supplemental Fig. S5. The normalized aggregate $PM_{2.5}$ mass monotonically increases as a function of RH for all three proxy samples. The Fajardo samples contain the greatest fraction of sodium and chloride ions (29.3% of the total mass), which drives its mass growth, with a mass at 55% RH of 1.09-1.12 times the mass at 35% RH. In contrast, the Abu Dhabi samples are mostly comprised of the medium growth component (58.5%, mostly ammonium and sulfate ions) with a corresponding growth of 1.03. The Bujumbura samples are predominantly comprised of low growth component (71.2%, treated as organic) with a corresponding growth of 1.011 to 1.012.

https://doi.org/10.5194/egusphere-2026-3224
Preprint. Discussion started: 22 June 2026

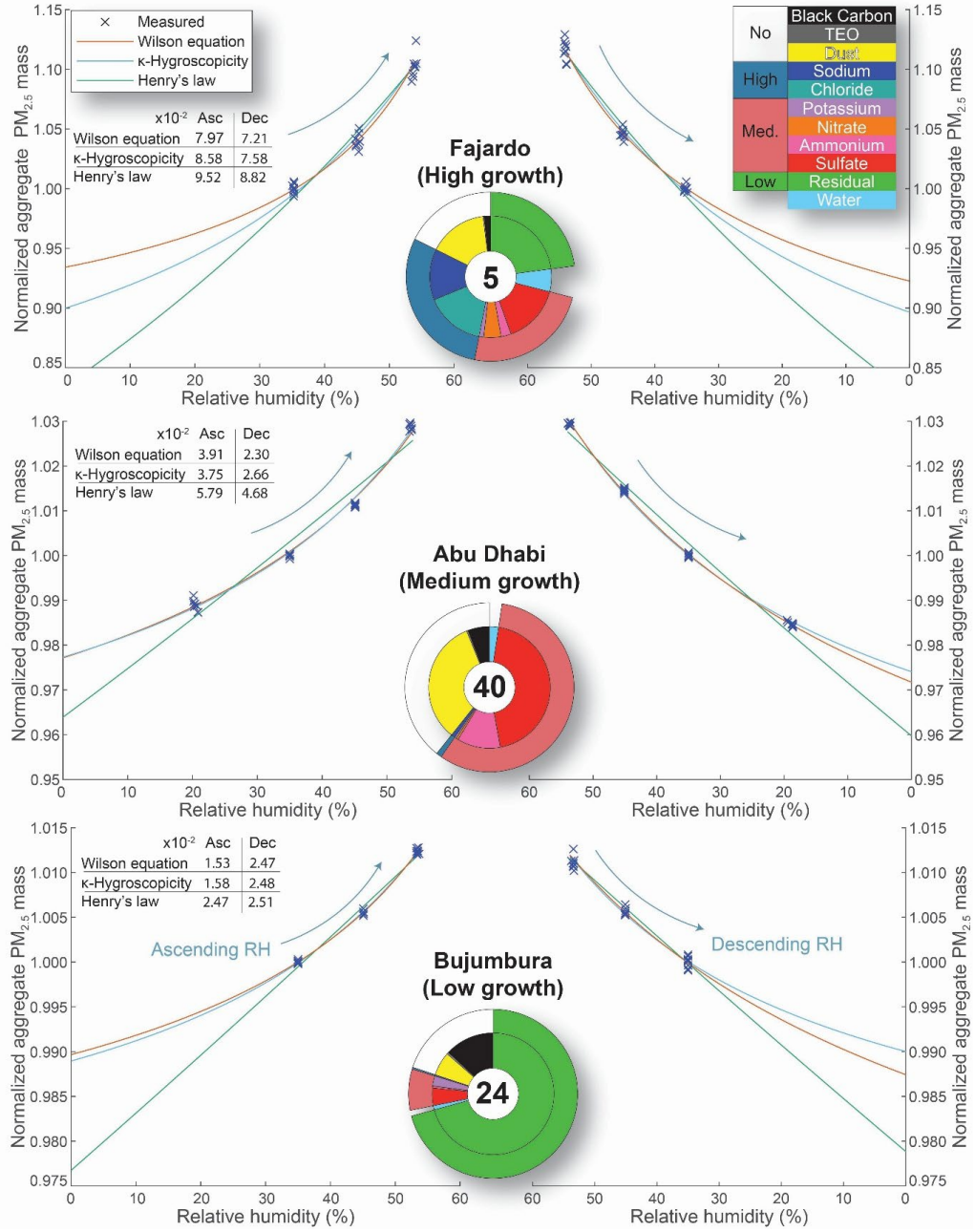

Figure 2. $PM_{2.5}$ mass as a function of ascending and descending RH with measured composition. Blue crosses indicate normalized $PM_{2.5}$ aggregate mass at elevated RH's beginning temporally at 20% or 35% (left panels) and 53% (right panels). Normalization uses the average mass at 35% RH. All normalization is done after calculations for graphing purposes only. Solid lines indicate the three fitted activity models. The normalized root mean square difference of each activity fit is shown in the tables. The inner pie charts display the measured aggregate composition of the filters measured. The outer ring of the pie charts displays which growth category the composition is assigned to high, medium, low, or no growth categories. The number in the center of the pie chart records the $PM_{2.5}$ mass concentration in $\mu g/m^3$ at 35% RH.

https://doi.org/10.5194/egusphere-2026-3224
Preprint. Discussion started: 22 June 2026

We fit the normalized mass with three activity models: Wilson equation, kappa-hygroscopicity, and Henry's law. Of the three activity models, the two-parameter Wilson equation generally best represents the growth in normalized aggregate mass as a function of RH, with the lowest normalized root mean square difference for both ascending and descending branches for all three proxy samples. We use the Wilson equation in the remainder of the study to extrapolate the gravimetric response to 0% RH. The disparity between samples in hygroscopic growth is apparent in the extrapolation too. The Fajardo $PM_{2.5}$ sample contains 6% to 7.5% water at 35% RH (1 - y-intercept). This water mass is 2 to 3 times the estimated water mass of the Abu Dhabi sample and 5 to 6 times the estimated water mass of the Bujumbura sample.

3.2. Water mass response of chemical categories

We use the Wilson activity models in Fig. 2, along with the composition, to attribute the water mass to the three growth categories. We assume that each of the growth categories independently absorbs water and is subject to its own Wilson equation. The Wilson equations for each category define the category's mass growth as a function of RH, and the sum of these three growth categories equals the fitted Wilson equation models in Fig. 2.

Table 4. The solved water fraction for the growth categories at three RH's. The numbers in parentheses are the 95% confidence interval (CI) at 35% RH. A-N-S-K represents Ammonium-Nitrate-Sulfate-Potassium.

Category	**Water content (fraction)**		
	35% (95% CI)	**45%**	**55%**
High growth (NaCl)	0.165 (0.116-0.265)	0.248	0.361
Medium growth (A-N-S-K)	0.039 (0.03-0.042)	0.057	0.08
Low growth (Residual as Organic)	0.0103 (0.006-0.013)	0.015	0.022

Table 4 shows the fraction of water for the growth categories at three RH's. The high growth category absorbs/adsorbs significantly more water (3.7 times) than the medium growth category and 16.2 times the low growth category. The 95% confidence interval for the high growth category is also significantly larger reflecting the spread of the data in the top panel of Fig. 2. Table 2 shows that the Fajardo samples have a much lower net mass than the other two samples which is the root cause of the increased variation. Supplemental text S6 explains how the confidence interval is calculated for each category. Equation 4 describes application of the

https://doi.org/10.5194/egusphere-2026-3224
Preprint. Discussion started: 22 June 2026

fractional of water $f_w(RH)$ from Table 4 to calculate the water mass (M_W) at a specified RH from the summed high growth (M_{HG}), medium growth (M_{MG}), and low growth (M_{LG}) masses.

$$M_W = M_{HG} * f_w(RH)_{HG} + M_{MG} * f_w(RH)_{MG} + M_{LG} * f_w(RH)_{LG} \quad (4)$$

3.3. Predicting two test cases and pure aerosol measurements

We now apply Equation 4 to predict the hygroscopic response for two test sites: Beijing and Halifax. The two test cases are compositionally different than the proxies. The Beijing sample (left panel in Figure 3) contains much more nitrate (12%) than the other sites. The Halifax sample (right panel) is primarily organic, similar to Bujumbura, but with the smallest amount of no-growth category (10%) in the study. The larger measurement variation at the test sites reflects a reduced number of measurements contributing to the aggregate (Table 3), and that the Halifax sample has a lower aggregate mass (Table 2). The Halifax data only includes the descending data as equipment failure compromised the ascending data.

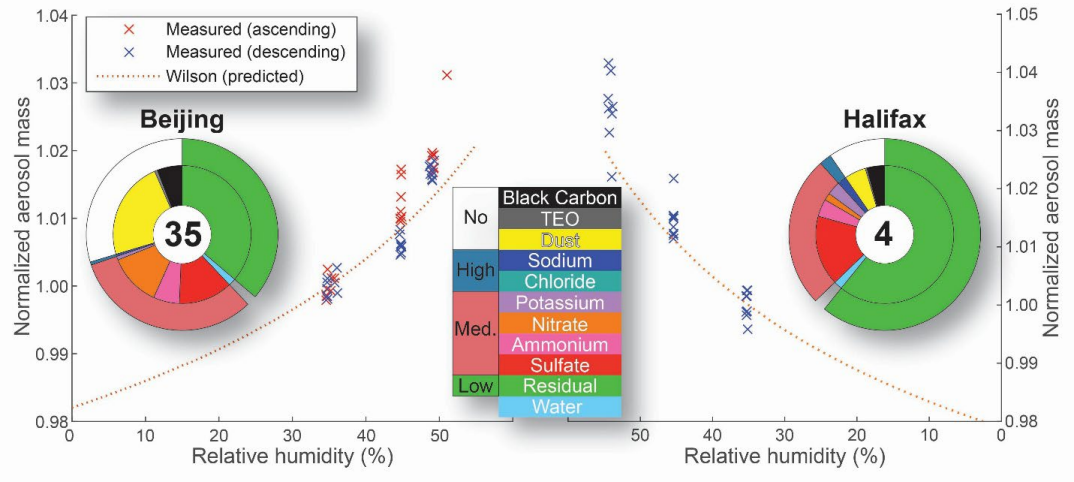

Figure 3. $PM_{2.5}$ mass as a function of ascending (red x's) and descending RH (blue x's) with measured composition. The dotted orange line is the predicted response from the solution in Table 3. The left panel shows the gravimetric response of $PM_{2.5}$ sampled in Beijing while Halifax is shown on the right. The inner pie charts display the measured aggregate composition. The outer ring of the pie chart displays which category the composition is assigned: high, medium, low, or no growth. The number in the center of the pie chart displays the $PM_{2.5}$ concentration in μg/m^3 at 35% RH. No ascending measurements are available for the Halifax sample.

The prediction (orange dotted line) generally represents the measurements with a normalized mean bias of 0.24% over both sites. The Beijing prediction is 0.45% below the average of the measurements at 50% RH but within 2 standard deviations. The effectiveness of

https://doi.org/10.5194/egusphere-2026-3224
Preprint. Discussion started: 22 June 2026

the Beijing prediction reflects the similar hygroscopic growth between nitrate and sulfate species (Petters and Kreidenweis, 2007). The Halifax prediction is also low by 0.40% at 50% RH.

We compared our results to prior measurements of water fraction in lab generated sea salt and ammonium sulfate on PTFE filters (Mcinnes et al., 1996) (Supplemental Table S3). The predictions of water associated with sea salt at 40% RH were low compared to the measurements but the two distributions overlap. The predictions of water associated with ammonium sulfate at 40% RH were consistent with the measurements.

3.4. Uncertainties

The extrapolation of the water activity to an RH of 0% may be subject to error due to diffusion limitations in the particles. If true, this diffusion limitation would create a higher apparent dry fraction for the descending experiment due to diffusivity decreasing with each decrease in RH (Koop et al., 2011). This trend is the opposite of what is observed in Fig. 2. The y-intercepts for the right panels (Wilson equation-descending) in Fig. 2 are usually lower than the y-intercepts in the left panel (Wilson equation-ascending). Thus, it appears unlikely that the measurements are subject to significant diffusional limitations for the 24 hour equilibration time used here.

We assume the water fraction to be zero when the RH is zero. Water could be incorporated into the crystalline structure of the salts themselves (hydrates) (Tobon et al., 2021). Water of crystallization may be stable over the range of RH (Kelly and Wexler, 2005). Thus, if there is stable water of crystallization over the investigated RH range, it will add to the water fraction estimated by this method.

Any ionic species (e.g. nitrate) that evaporates during the hygroscopicity experiment cannot be measured later by ion chromatography, which occurred after the hygroscopicity experiment. Over the course of the experiment, 2.9% of the total mass evaporated from the Fajardo filters, 1.2% from the Abu Dhabi filters, and 0.7% from the Bujumbura filters. These are total masses that could include other species besides volatile ionic species. Additionally, these percentages are on the order of (Abu Dhabi and Bujumbura) or smaller than (Fajardo) the confidence intervals shown in Table 4. It is infeasible to isolate the impact of that small mass on our results given the uncertainty in Table 4.

https://doi.org/10.5194/egusphere-2026-3224
Preprint. Discussion started: 22 June 2026

3.5. Application of the model to SPARTAN

Figure 4 shows the average composition of the 24 sites in this study. A tabulated version of these compositions is in Supplemental Table S4. The low growth category, treated as organic, on average comprises the largest fraction (37%) across the network. Bujumbura, Burundi, the low growth proxy, contains the largest fraction of low growth category (70%). Five (Bujumbura, Sherbrooke, Norman, Bandung, and Halifax) of the 24 sites have a low growth category fraction of over 50%. The medium growth category is the second largest (29%) reflecting the abundance of ammonium, nitrate, sulfate, and potassium. Abu Dhabi, the medium growth proxy, has the largest fraction of medium growth component (51%). The no-growth category is also approximately 29% by mass. The largest no-growth category sites (Ilorin, Abu Dhabi, Addis Ababa, Dhaka, and Fajardo) are heavily influenced by mineral dust. The Dhaka site is also significantly influenced by TEO (Liu et al., 2024). The high growth category (NaCl) is the smallest fraction (3.2%). Fajardo, the high growth proxy, has the largest fraction of sodium chloride. Other coastal sites (Melbourne, Halifax, Taipei) contain a significant fraction of the high growth category. An exception is Delhi, which has significant chloride content without sodium (Manchanda et al., 2022).

The outer pie charts in Fig. 4 show the water content at 35% RH predicted using the categories in Table 4. A tabulated form is in Table S6. The average inferred water content for the 24 sites in SPARTAN is 2.1%. This water content varies from 0.9% in Ilorin, Nigeria (the site with the largest no growth category) to 5.5% in Fajardo, Puerto Rico (the site with the largest high growth category). The medium growth category dominates, contributing 58% of the water across the entire network. Organics (low growth) follow at 22% with the high growth category contributing just 19% of the total water mass. Samples with the highest water content are coastal.

https://doi.org/10.5194/egusphere-2026-3224
Preprint. Discussion started: 22 June 2026

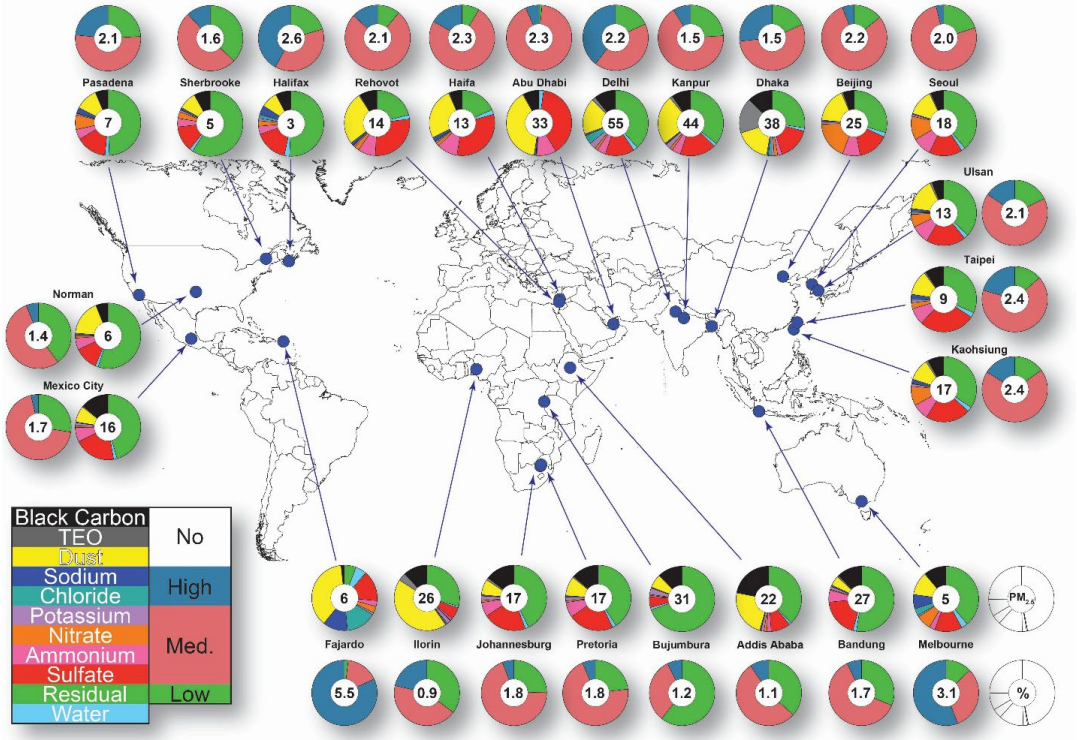

Figure 4. Water content and composition for SPARTAN over December 2019 through September 2024. The inside ring of pie charts documents the mass concentration and $PM_{2.5}$ composition. The $PM_{2.5}$ concentrations are the inner circle ($\mu g/m^3$), and the chemical composition (filled colors) surround the mass concentration. The outside ring of pie charts documents the water content. The water content is in the inner circle (%), and the contributions of the three categories surround the water content.

This water content prediction may contain some error when applied to specific sites. For example, the chloride in Delhi may not be best represented by the chloride content from the coastal Puerto Rico proxy. Additionally, the trace element oxide content in Dhaka is treated as hydrophobic (no growth). There is little published evidence on the hygroscopicity of trace element oxides.

Nitrate is known to evaporate from PTFE filters such as those used in this study (Hering and Cass, 1999; Chow et al., 2015; Ashbaugh and Eldred, 2004; Shaw et al., 1982). SPARTAN sampling station inlets were retrofitted with an MgO denuder, and a nylon filter placed after the PTFE filter to address this issue, beginning on 1/1/2025. This development will be described elsewhere. The additional nitrate associated with the nylon filter does not affect absolute water content on PTFE filters.

https://doi.org/10.5194/egusphere-2026-3224
Preprint. Discussion started: 22 June 2026

4. Conclusions

Overall, this study determined the composition dependent water content on PTFE filters at low relative humidity for a globally-dispersed network of sites as a part of SPARTAN. An empirical relationship was developed to predict the water mass due to $PM_{2.5}$ composition at RH below 55% as a function of three chemical categories. The Wilson equation (Wilson, 1964) was the activity model that best represented measured water mass. The high growth category containing the sum of the mass of sodium and chloride had a water fraction at 35% RH of 0.165 (0.116 – 0.265, 95% confidence). The medium growth category containing the sum of the mass of ammonium, nitrate, sulfate, and potassium had a water fraction at 35% RH of 0.039 (0.03 – 0.042, 95% confidence). The low growth category contained organics and had a water fraciton at 35% RH of 0.0103 (0.006 – 0.013, 95% confidence). The water fraction at 45% was 1.5 times that at 35% RH, indicating sensitivity to other network protocols. The created relationship predicted the water content of both pure component aerosols and two independent test sites: Beijing, China (within 0.16%) and Halifax, Canada (within 0.40%). Thus, the relationship successfully predicted the water mass/RH relationship of 5 globally distributed sites, each with disparate composition.

Application of the relationship to SPARTAN over the period of December 2019 through September 2024 yielded an estimated average water content at 35% RH for the entire network of 2.1%, ranging from 0.9% at Illorin, Nigeria to 5.5% Fajardo, Puerto Rico. The medium growth category contributed 58% of the water content on average while the low and high growth category contributed 22% and 19% respectively. The empirical relationship developed in this study offer a straight-forward method to accurately calculate $PM_{2.5}$ water content on PTFE filters below 55% RH which is useful for both mass reconstruction algorithms and chemical transport models.

Code/Data availability: Hygroscopicity experimental data and scripts are available upon request. All composition data is available from www.spartan-network.org. Scripts used to create the data posted on the website are available upon request.

Author Contributions: CRO and RVM conceptualized the project and wrote the manuscript. CRO wrote the analysis software and performed the formal analysis. The water content experimental methodology was developed by CRO and MM. The image based reflectance methodology was setup by MA. AMD managed FTIR and HIPS analysis for all samples. Setup and collection of samples for the investigation was made by IAA, TBA, CA, OAM, CJF, RMG, SH, FI, KL, TM,

https://doi.org/10.5194/egusphere-2026-3224
Preprint. Discussion started: 22 June 2026

MN, NN, BS, RS, EKW, EW. Document editing by TS. Laboratory analysis was performed by CRO, MM, XL, YxR, and MA. Software for consolidation of chemical composition information was programmed by HZ. Supervision of individual sites made by IAA, TBA, AA, RYWC, SD, DJD, CJF, DF, PG, RMG, MG, JK, KL, PCL, PL, PHL, SMLS, OLMB, SSP, AS, BS, RS, YS, SNT, MTW, YR QZ. Management of network by MB, YR, JRT, and RVM.

Competing Interests: At least one of the (co-)authors is a member of the editorial board of Atmospheric Measurement Techniques.

Acknowledgements

This work was supported by the Clean Air Fund 001591 (RVM), NASA Grant 80NSSC21K0508 (RVM), and NSF Grant 2020673 (RVM), with additional contributions from NASA and the US Agency for International Development via the MAIA project. The work of SH and DJD was carried out at the Jet Propulsion Laboratory, California Institute of Technology, under a contract with NASA (80NM0018D0004). SD acknowledges the research grant from the Clean Air Fund (001307) to IIT Delhi. PCL is partly supported by the National Health Research Institutes (NHRI-EX114-11410PI).

References

Abbey, D. E., Burchette, R. J., Knutsen, S. F., McDonnell, W. F., Lebowitz, M. D., and Enright, P. L.: Long-term particulate and other air pollutants and lung function in nonsmokers, Am. J. Respir. Crit. Care Med., 158, 289–298, 10.1164/ajrccm.158.1.9710101, 1998.

Abbey, D. E., Nishino, N., McDonnell, W. F., Burchette, R. J., Knutsen, S. F., Beeson, W. L., and Yang, J. X.: Long-term inhalable particles and other air pollutants related to mortality in nonsmokers, Am. J. Respir. Crit. Care Med., 159, 373–382, 10.1164/ajrccm.159.2.9806020, 1999.

Ashbaugh, L. and Eldred, R.: Loss of particle nitrate from Teflon sampling filters: Effects on measured gravimetric mass in California and in the IMPROVE network, J. Air Waste Manage. Assoc., 54, 93–104, 10.1080/10473289.2004.10470878, 2004.

Babela, D. and Lamorena, R. B.: Effect of humidity and organic vapors on water absorption of metal oxides, Chem. Pap., 74, 217–227, 10.1007/s11696-019-00870-2, 2020.

Brook, R. D., Rajagopalan, S., Pope, C. A., Brook, J. R., Bhatnagar, A., Diez-Roux, A. V., Holguin, F., Hong, Y. L., Luepker, R. V., Mittleman, M. A., Peters, A., Siscovick, D., Smith, S. C.,

https://doi.org/10.5194/egusphere-2026-3224
Preprint. Discussion started: 22 June 2026

667 Whitsel, L., Kaufman, J. D., Amer Heart Assoc Council, E., Council Kidney Cardiovasc, D., and
668 Council Nutr Phys Activity, M.: Particulate Matter Air Pollution and Cardiovascular Disease An
669 Update to the Scientific Statement From the American Heart Association, Circulation, 121,
670 2331–2378, 10.1161/CIR.0b013e3181dbece1, 2010.

671 Canepari, S., Simonetti, G., and Perrino, C.: Mass size distribution of particle-bound water,
672 Atmos. Environ., 165, 46–56, 10.1016/j.atmosenv.2017.06.034, 2017.

673 Canepari, S., Farao, C., Marconi, E., Giovannelli, C., and Perrino, C.: Qualitative and
674 quantitative determination of water in airborne particulate matter, Atmos. Chem. Phys., 13,
675 1193–1202, 10.5194/acp-13-1193-2013, 2013.

676 Chen, L. X. D., Peng, C., Gu, W. J., Fu, H. J., Jian, X., Zhang, H. H., Zhang, G. H., Zhu, J. X.,
677 Wang, X. M., and Tang, M. J.: On mineral dust aerosol hygroscopicity, Atmos. Chem. Phys., 20,
678 13611–13626, 10.5194/acp-20-13611-2020, 2020.

679 Chow, J. C. and Watson, J. G.: Ion chromatography in elemental analysis of airborne particles,
680 in: Elemental analysis of airborne particles, edited by: Landsberger, S., and Creatchman, M.,
681 Gordon and Breach Science Publishers, Amsterdam, Netherlands, 97–137, 1999.

682 Chow, J. C., Lowenthal, D. H., Chen, L. W. A., Wang, X., and Watson, J. G.: Mass
683 reconstruction methods for PM2.5: a review, Air Quality, Atmosphere & Health, 8, 243–263,
684 10.1007/s11869-015-0338-3, 2015.

685 Chow, J. C., Watson, J. G., Pritchett, L. C., Pierson, W. R., Frazier, C. A., and Purcell, R. G.:
686 The DRI Thermal Optical Reflectance Carbon Analysis System - Description, Evaluation and
687 Applications in United States Air Quality, Atmospheric Environment Part a-General Topics, 27,
688 1185–1201, 10.1016/0960-1686(93)90245-t, 1993a.

689 Chow, J. C., Watson, J. G., Pritchett, L. C., Pierson, W. R., Frazier, C. A., and Purcell, R. G.:
690 THE DRI THERMAL OPTICAL REFLECTANCE CARBON ANALYSIS SYSTEM -
691 DESCRIPTION, EVALUATION AND APPLICATIONS IN UNITED-STATES AIR-QUALITY
692 STUDIES, Atmospheric Environment Part a-General Topics, 27, 1185–1201, 10.1016/0960-
693 1686(93)90245-t, 1993b.

694 Dabek-Zlotorzynska, E., Dann, T. F., Martinelango, P. K., Celo, V., Brook, J. R., Mathieu, D.,
695 Ding, L. Y., and Austin, C. C.: Canadian National Air Pollution Surveillance (NAPS) PM2.5
696 speciation program: Methodology and PM2.5 chemical composition for the years 2003-2008,
697 Atmos. Environ., 45, 673–686, 10.1016/j.atmosenv.2010.10.024, 2011.

698 Daellenbach, K. R., Bozzetti, C., Krepelová, A. K., Canonaco, F., Wolf, R., Zotter, P., Fermo, P.,
699 Crippa, M., Slowik, J. G., Sosedova, Y., Zhang, Y., Huang, R. J., Poulain, L., Szidat, S.,
700 Baltensperger, U., El Haddad, I., and Prévôt, A. S. H.: Characterization and source
701 apportionment of organic aerosol using offline aerosol mass spectrometry, Atmos. Meas. Tech.,
702 9, 23–39, 10.5194/amt-9-23-2016, 2016.

703 Debus, B., Weakley, A., Takahama, S., George, K., Amiri-Farahani, A., Schichtel, B., Copeland,
704 S., Wexler, A., and Dillner, A.: Quantification of major particulate matter species from a single
705 filter type using infrared spectroscopy - application to a large-scale monitoring network, Atmos.
706 Meas. Tech., 15, 2685–2702, 10.5194/amt-15-2685-2022, 2022.

https://doi.org/10.5194/egusphere-2026-3224
Preprint. Discussion started: 22 June 2026

Devres, Y. O.: Psychrometric Properties of Humid Air - Calculation Procedures, Appl. Energy, 48, 1–18, 10.1016/0306-2619(94)90063-9, 1994.

Dillner, A. and Takahama, S.: Predicting ambient aerosol thermal-optical reflectance (TOR) measurements from infrared spectra: organic carbon, Atmos. Meas. Tech., 8, 1097–1109, 10.5194/amt-8-1097-2015, 2015.

Diner, D. J., Boland, S. W., Brauer, M., Bruegge, C., Burke, K. A., Chipman, R., Di Girolamo, L., Garay, M. J., Hasheminassab, S., Hyer, E., Jerrett, M., Jovanovic, V., Kalashnikova, O. V., Liu, Y., Lyapustin, A. I., Martin, R. V., Nastan, A., Ostro, B. D., Ritz, B., Schwartz, J., Wang, J., and Xu, F.: Advances in multiangle satellite remote sensing of speciated airborne particulate matter and association with adverse health effects: from MISR to MAIA, J. Appl. Remote Sens., 12, 22, 10.1117/1.Jrs.12.042603, 2018.

Dockery, D. W., Pope, C. A., Xu, X. P., Spengler, J. D., Ware, J. H., Fay, M. E., Ferris, B. G., and Speizer, F. E.: An Association Between Air Pollution and Mortality in 6 United States Cities, N. Engl. J. Med., 329, 1753–1759, 10.1056/nejm199312093292401, 1993.

Fischer, K.: A new method for the analytical determination water in liquids and solids, Angew. Chem., 48, 0394–0396, 10.1002/ange.19350482605, 1935.

Hering, S. and Cass, G.: The magnitude of bias in the measurement of PM2.5 arising from volatilization of particulate nitrate from teflon filters, J. Air Waste Manage. Assoc., 49, 725–733, 10.1080/10473289.1999.10463843, 1999.

Holben, B., Eck, T., Slutsker, I., Tanre, D., Buis, J., Setzer, A., Vermote, E., Reagan, J., Kaufman, Y., Nakajima, T., Lavenu, F., Jankowiak, I., and Smirnov, A.: AERONET - A federated instrument network and data archive for aerosol characterization, Remote Sens. Environ., 66, 1–16, 10.1016/s0034-4257(98)00031-5, 1998.

Hong, J., Häkkinen, S. A. K., Paramonov, M., Äijälä, M., Hakala, J., Nieminen, T., Mikkilä, J., Prisle, N. L., Kulmala, M., Riipinen, I., Bilde, M., Kerminen, V. M., and Petäjä, T.: Hygroscopicity, CCN and volatility properties of submicron atmospheric aerosol in a boreal forest environment during the summer of 2010, Atmos. Chem. Phys., 14, 4733–4748, 10.5194/acp-14-4733-2014, 2014.

Jeronimo, M., Stewart, Q., Weakley, A. T., Giacomo, J., Zhang, X. L., Hyslop, N., Dillner, A. M., Shupler, M., and Brauer, M.: Analysis of black carbon on filters by image-based reflectance, Atmos. Environ., 223, 8, 10.1016/j.atmosenv.2020.117300, 2020.

Kazemiparkouhi, F., Honda, T., Eum, K. D., Wang, B. Y., Manjourides, J., and Suh, H. H.: The impact of Long-Term PM_{2.5} constituents and their sources on specific causes of death in a US Medicare cohort, Environ. Int., 159, 11, 10.1016/j.envint.2021.106988, 2022.

Kelly, J. and Wexler, A.: Thermodynamics of carbonates and hydrates related to heterogeneous reactions involving mineral aerosol, J. Geophys. Res.-Atmos., 110, 13, 10.1029/2004jd005583, 2005.

Koop, T., Bookhold, J., Shiraiwa, M., and Pöschl, U.: Glass transition and phase state of organic compounds: dependency on molecular properties and implications for secondary organic

https://doi.org/10.5194/egusphere-2026-3224
Preprint. Discussion started: 22 June 2026

746 aerosols in the atmosphere, Phys. Chem. Chem. Phys., 13, 19238–19255,
747 10.1039/c1cp22617g, 2011.

748 Lipfert, F. W., Malone, R. G., Daum, M. L., Mendell, N. R., and Yang, C.: A Statisitical Study of
749 the Macroepidemiology of Air Pollution and Total Mortality, Brookhaven National Laboratory,
750 Upton, NY, 1988.

751 Liu, X., Turner, J. R., Hand, J. L., Schichtel, B. A., and Martin, R.: A Global-Scale Mineral Dust
752 Equation, J. Geophys. Res.-Atmos., 127, 22, 10.1029/2022jd036937, 2022.

753 Liu, X., Turner, J. R., Oxford, C. R., McNeill, J., Walsh, B., Le Roy, E., Weagle, C. L., Stone, E.,
754 Zhu, H., Liu, W., Wei, Z., Hyslop, N. P., Giacomo, J., Dillner, A. M., Salam, A., Hossen, A.-a.,
755 Islam, Z., Abboud, I., Akoshile, C., Amador-Muñoz, O., Anh, N. X., Asfaw, A., Balasubramanian,
756 R., Chang, R. Y.-W., Coburn, C., Dey, S., Diner, D. J., Dong, J., Farrah, T., Gahungu, P.,
757 Garland, R. M., Grutter de la Mora, M., Hasheminassab, S., John, J., Kim, J., Kim, J. S.,
758 Langerman, K., Lee, P.-C., Lestari, P., Liu, Y., Mamo, T., Martins, M., Mayol-Bracero, O. L.,
759 Naidoo, M., Park, S. S., Schechner, Y., Schofield, R., Tripathi, S. N., Windwer, E., Wu, M.-T.,
760 Zhang, Q., Brauer, M., Rudich, Y., and Martin, R. V.: Elemental Characterization of Ambient
761 Particulate Matter for a Globally Distributed Monitoring Network: Methodology and Implications,
762 ACS ES&T Air, 1, 283–293, 10.1021/acsestair.3c00069, 2024.

763 Manchanda, C., Kumar, M., and Singh, V.: Meteorology governs the variation of Delhi's high
764 particulate-bound chloride levels, Chemosphere, 291, 8, 10.1016/j.chemosphere.2021.132879,
765 2022.

766 Martin, M., Chang, R. Y. W., Sierau, B., Sjogren, S., Swietlicki, E., Abbatt, J. P. D., Leck, C., and
767 Lohmann, U.: Cloud condensation nuclei closure study on summer arctic aerosol, Atmos. Chem.
768 Phys., 11, 11335–11350, 10.5194/acp-11-11335-2011, 2011.

769 McInnes, L. M., Quinn, P. K., Covert, D. S., and Anderson, T. L.: Gravimetric analysis, ionic
770 composition, and associated water mass of the marine aerosol, Atmos. Environ., 30, 869–884,
771 10.1016/1352-2310(95)00354-1, 1996.

772 McMurry, P., Litchy, M., Huang, P., Cai, X., Turpin, B., Dick, W., and Hanson, A.: Elemental
773 composition and morphology of individual particles separated by size and hygroscopicity with
774 the TDMA, Atmos. Environ., 30, 101–108, 10.1016/1352-2310(95)00235-q, 1996.

775 McNeill, J., Snider, G., Weagle, C., Walsh, B., Bissonnette, P., Stone, E., Abboud, I., Akoshile,
776 C., Anh, N., Balasubramanian, R., Brook, J., Coburn, C., Cohen, A., Dong, J., Gagnon, G.,
777 Garland, R., He, K., Holben, B., Kahn, R., Kim, J., Lagrosas, N., Lestari, P., Liu, Y., Jeba, F., Joy,
778 K., Martins, J., Misra, A., Norford, L., Quel, E., Salam, A., Schichtel, B., Tripathi, S., Wang, C.,
779 Zhang, Q., Brauer, M., Gibson, M., Rudich, Y., and Martin, R.: Large global variations in
780 measured airborne metal concentrations driven by anthropogenic sources, Sci Rep, 10, 12,
781 10.1038/s41598-020-78789-y, 2020.

782 Mikhailov, E., Vlasenko, S., Rose, D., and Pöschl, U.: Mass-based hygroscopicity parameter
783 interaction model and measurement of atmospheric aerosol water uptake, Atmos. Chem. Phys.,
784 13, 717–740, 10.5194/acp-13-717-2013, 2013.

https://doi.org/10.5194/egusphere-2026-3224
Preprint. Discussion started: 22 June 2026

Noble, C., Vanderpool, R., Peters, T., McElroy, F., Gemmill, D., and Wiener, R.: Federal reference and equivalent methods for measuring fine particulate matter, Aerosol Sci. Technol., 34, 457–464, 10.1080/027868201750172914, 2001.

Pandey, A., Shetty, N., and Chakrabarty, R.: Aerosol light absorption from optical measurements of PTFE membrane filter samples: sensitivity analysis of optical depth measures, Atmos. Meas. Tech., 12, 1365–1373, 10.5194/amt-12-1365-2019, 2019.

Petters, M. D. and Kreidenweis, S. M.: A single parameter representation of hygroscopic growth and cloud condensation nucleus activity, Atmos. Chem. Phys., 7, 1961–1971, 10.5194/acp-7-1961-2007, 2007.

Pope, C. A., Burnett, R. T., Thurston, G. D., Thun, M. J., Calle, E. E., Krewski, D., and Godleski, J. J.: Cardiovascular mortality and long-term exposure to particulate air pollution - Epidemiological evidence of general pathophysiological pathways of disease, Circulation, 109, 71–77, 10.1161/01.Cir.0000108927.80044.7f, 2004.

Pope, C. A., Thun, M. J., Namboodiri, M. M., Dockery, D. W., Evans, J. S., Speizer, F. E., and Heath, C. W.: Particulate Air Pollution as a Predictor of Mortality in a Prospective Study of US Adults, Am. J. Respir. Crit. Care Med., 151, 669–674, 1995.

Rees, S. L., Robinson, A. L., Khlystov, A., Stanier, C. O., and Pandis, S. N.: Mass balance closure and the federal reference method for PM_{2.5} in Pittsburgh, Pennsylvania, Atmos. Environ., 38, 3305–3318, 10.1016/j.atmosenv.2004.03.016, 2004.

Reggente, M., Dillner, A., and Takahama, S.: Predicting ambient aerosol thermal-optical reflectance (TOR) measurements from infrared spectra: extending the predictions to different years and different sites, Atmos. Meas. Tech., 9, 441–454, 10.5194/amt-9-441-2016, 2016.

Register, A. C. o. t. F.: Reference Method for the Determination of Fine Particulate Matter as PM2.5 in the Atmosphere, 2020.

Ren, Y., Oxford, C., Zhang, D., Liu, X., Zhu, H., Dillner, A., White, W., Chakrabarty, R., Hasheminassab, S., Diner, D., Le Roy, E., Kumar, J., Viteri, V., Song, K., Akoshile, C., Amador-Muñoz, O., Asfaw, A., Chang, R., Francis, D., Gahungu, P., Garland, R., Grutter, M., Kim, J., Langerman, K., Lee, P., Lestari, P., Mayol-Bracero, O., Naidoo, M., Nelli, N., O'Neill, N., Park, S., Salam, A., Sarangi, B., Schechner, Y., Schofield, R., Tripathi, S., Windwer, E., Wu, M., Zhang, Q., Rudich, Y., Brauer, M., and Martin, R.: Black carbon emissions generally underestimated in the global south as revealed by globally distributed measurements, Nat. Commun., 16, 9, 10.1038/s41467-025-62468-5, 2025.

Ruthenburg, T. C., Perlin, P. C., Liu, V., McDade, C. E., and Dillner, A. M.: Determination of organic matter and organic matter to organic carbon ratios by infrared spectroscopy with application to selected sites in the IMPROVE network, Atmos. Environ., 86, 47–57, 10.1016/j.atmosenv.2013.12.034, 2014.

Shaw, R., Stevens, R., Bowermaster, J., Tesch, J., and Tew, E.: Measurements of Atmospheric Nitrate and Nitric Acid - The Denuder Difference Experiment, Atmos. Environ., 16, 845–853, 10.1016/0004-6981(82)90403-6, 1982.

https://doi.org/10.5194/egusphere-2026-3224
Preprint. Discussion started: 22 June 2026

Snider, G., Weagle, C. L., Martin, R. V., van Donkelaar, A., Conrad, K., Cunningham, D., Gordon, C., Zwicker, M., Akoshile, C., Artaxo, P., Anh, N. X., Brook, J., Dong, J., Garland, R. M., Greenwald, R., Griffith, D., He, K., Holben, B. N., Kahn, R., Koren, I., Lagrosas, N., Lestari, P., Ma, Z., Martins, J. V., Quel, E. J., Rudich, Y., Salam, A., Tripathi, S. N., Yu, C., Zhang, Q., Zhang, Y., Brauer, M., Cohen, A., Gibson, M. D., and Liu, Y.: SPARTAN: a global network to evaluate and enhance satellite-based estimates of ground-level particulate matter for global health applications, Atmos. Meas. Tech., 8, 505–521, 10.5194/amt-8-505-2015, 2015.

Snider, G., Weagle, C. L., Murdymootoo, K. K., Ring, A., Ritchie, Y., Stone, E., Walsh, A., Akoshile, C., Anh, N. X., Balasubramanian, R., Brook, J., Qonitan, F. D., Dong, J. L., Griffith, D., He, K. B., Holben, B. N., Kahn, R., Lagrosas, N., Lestari, P., Ma, Z. W., Misra, A., Norford, L. K., Quel, E. J., Salam, A., Schichtel, B., Segev, L., Tripathi, S., Wang, C., Yu, C., Zhang, Q., Zhang, Y. X., Brauer, M., Cohen, A., Gibson, M. D., Liu, Y., Martins, J. V., Rudich, Y., and Martin, R. V.: Variation in global chemical composition of PM2.5: emerging results from SPARTAN, Atmos. Chem. Phys., 16, 9629–9653, 10.5194/acp-16-9629-2016, 2016.

Speer, R. E., Edney, E. O., and Kleindienst, T. E.: Impact of organic compounds on the concentrations of liquid water in ambient PM_{2.5}, J. Aerosol. Sci., 34, 63–77, 10.1016/s0021-8502(02)00152-0, 2003.

Spengler, J. D. and Thurston, G. D.: Mass and Elemental Composition of Fine and Coarse Particles in 6 United States Cities, Journal of the Air Pollution Control Association, 33, 1162–1171, 10.1080/00022470.1983.10465707, 1983.

Standardization, E. C. f.: Ambient air – Standard gravimetric measurement method for the determination of the PM10 or PM2,5 mass concentration of suspended particulate matter, 2023.

Su, Z. Y., Chen, L. X. D., Liu, Y., Zhang, P., Chen, T. Z., Chu, B. W., Tang, M. J., Ma, Q. X., and He, H.: A study on the influence of inorganic ions, organic carbon and microstructure on the hygroscopic property of soot, Atmos. Chem. Phys., 24, 993–1003, 10.5194/acp-24-993-2024, 2024.

Surratt, J. D., Gómez-González, Y., Chan, A. W. H., Vermeylen, R., Shahgholi, M., Kleindienst, T. E., Edney, E. O., Offenberg, J. H., Lewandowski, M., Jaoui, M., Maenhaut, W., Claeys, M., Flagan, R. C., and Seinfeld, J. H.: Organosulfate formation in biogenic secondary organic aerosol, J. Phys. Chem. A, 112, 8345–8378, 10.1021/jp802310p, 2008.

Tang, I. N.: Thermodynamic and optical properties of mixed-salt aerosols of atmospheric importance, J. Geophys. Res.-Atmos., 102, 1883–1893, 10.1029/96jd03085, 1997.

Tang, M., Chan, C., Li, Y., Su, H., Ma, Q., Wu, Z., Zhang, G., Wang, Z., Ge, M., Hu, M., He, H., and Wang, X.: A review of experimental techniques for aerosol hygroscopicity studies, Atmos. Chem. Phys., 19, 12631–12686, 10.5194/acp-19-12631-2019, 2019a.

Tang, M. J., Zhang, H. H., Gu, W. J., Gao, J., Jian, X., Shi, G. L., Zhu, B. Q., Xie, L. H., Guo, L. Y., Gao, X. Y., Wang, Z., Zhang, G. H., and Wang, X. M.: Hygroscopic Properties of Saline Mineral Dust From Different Regions in China: Geographical Variations, Compositional Dependence, and Atmospheric Implications, J. Geophys. Res.-Atmos., 124, 10844–10857, 10.1029/2019jd031128, 2019b.

https://doi.org/10.5194/egusphere-2026-3224
Preprint. Discussion started: 22 June 2026

Tester, J. W. and Modell, M.: Thermodynamics and its applications, 3rd, Prentice-Hall international series in the physical and chemical engineering sciences, Prentice Hall PTR, Upper Saddle River, N.J., xviii, 936, I936 p. pp.1997.

Tobon, Y. A., El Hajj, D., Seng, S., Bengrad, F., Moreau, M., Visez, N., Chiapello, I., Crumeyrolle, S., and Choël, M.: Impact of the particle mixing state on the hygroscopicity of internally mixed sodium chloride-ammonium sulfate single droplets: a theoretical and experimental study, Phys. Chem. Chem. Phys., 23, 14391–14403, 10.1039/d1cp01574e, 2021.

van Donkelaar, A., Martin, R. V., Brauer, M., Kahn, R., Levy, R., Verduzco, C., and Villeneuve, P. J.: Global Estimates of Ambient Fine Particulate Matter Concentrations from Satellite-Based Aerosol Optical Depth: Development and Application, Environ. Health Perspect., 118, 847–855, 10.1289/ehp.0901623, 2010.

van Donkelaar, A., Hammer, M. S., Bindle, L., Brauer, M., Brook, J. R., Garay, M. J., Hsu, N. C., Kalashnikova, O. V., Kahn, R. A., Lee, C. L., Levy, R. C., Lyapustin, A., Sayer, A. M., and Martin, R. V.: Monthly Global Estimates of Fine Particulate Matter and Their Uncertainty, Environ. Sci. Technol., 58, 4463–4464, 10.1021/acs.est.4c01477, 2024.

Watson, J., Chow, J., and Frazier, C.: X-ray fluorescence analysis of ambient air samples, in: Elemental analysis of airborne particles, edited by: Landsberger, S., and Creatchman, M., Gordon and Breach Science Publishers, Amsterdam, Netherlands, 67–96, 1999.

Weagle, C. L., Snider, G., Li, C., van Donkelaar, A., Philip, S., Bissonnette, P., Burke, I., Jackson, J., Latimer, R., Stone, E., Abboud, I., Akoshile, C., Anh, N. X., Brook, J. R., Cohen, A., Dong, J. L., Gibson, M. D., Griffith, D., He, K. B., Holben, B. N., Kahn, R., Keller, C. A., Kim, J. S., Lagrosas, N., Lestari, P., Khian, Y. L., Liu, Y., Marais, E. A., Martins, J. V., Misra, A., Muliane, U., Pratiwi, R., Quel, E. J., Salam, A., Segey, L., Tripathi, S. N., Wang, C., Zhang, Q., Brauer, M., Rudich, Y., and Martin, R. V.: Global Sources of Fine Particulate Matter: Interpretation of PM2.5 Chemical Composition Observed by SPARTAN using a Global Chemical Transport Model, Environ. Sci. Technol., 52, 11670–11681, 10.1021/acs.est.8b01658, 2018.

Weingartner, E., Burtscher, H., and Baltensperger, U.: Hygroscopic properties of carbon and diesel soot particles, Atmos. Environ., 31, 2311–2327, 10.1016/s1352-2310(97)00023-x, 1997.

White, W. H., Trzepla, K., Hyslop, N. P., and Schichtel, B. A.: A critical review of filter transmittance measurements for aerosol light absorption, and de novo calibration for a decade of monitoring on PTFE membranes, Aerosol Sci. Technol., 50, 984–1002, 10.1080/02786826.2016.1211615, 2016.

Wilson, G. M.: Vapor-liquid equilibrium. XI. A new expression for the excess free energy of mixing, Journal of the American Chemical Society, 86, 127–130, 1964.

Wolf, K., Hoffmann, B., Andersen, Z. J., Atkinson, R. W., Bauwelinck, M., Bellander, T., Brandt, J., Brunekreef, B., Cesaroni, G., Chen, J., de Faire, U., de Hoogh, K., Fecht, D., Forastiere, F., Gulliver, J., Hertel, O., Hvidtfeldt, U. A., Janssen, N. A. H., Jorgensen, J. T., Katsouyanni, K., Ketzel, M., Klompmaker, J. O., Lager, A., Liu, S., MacDonald, C. J., Magnusson, P. K. E., Mehta, A. J., Nagel, G., Oftedal, B., Pedersen, N. L., Pershagen, G., Raaschou-Nielsen, O., Renzi, M., Rizzuto, D., Rodopoulou, S., Samoli, E., van der Schouw, Y. T., Schramm, S., Schwarze, P., Sigsgaard, T., Sorensen, M., Stafoggia, M., Strak, M., Tjonneland, A., Verschuren, W. M. M., Vienneau, D., Weinmayr, G., Hoek, G., Peters, A., and Ljungman, P. L. S.: Long-term exposure

https://doi.org/10.5194/egusphere-2026-3224
Preprint. Discussion started: 22 June 2026

907 to low-level ambient air pollution and incidence of stroke and coronary heart disease: a pooled
908 analysis of six European cohorts within the ELAPSE project, Lancet Planet. Health, 5, E620–
909 E632, 2021.

910 Yatkin, S., Trzepla, K., White, W., and Hyslop, N.: Generation of multi-element reference
911 materials on PTFE filters mimicking ambient aerosol characteristics, Atmos. Environ., 189, 41–
912 49, 10.1016/j.atmosenv.2018.06.034, 2018.

913 Zhong, M. and Jang, M.: Light absorption coefficient measurement of SOA using a UV-Visible
914 spectrometer connected with an integrating sphere, Atmos. Environ., 45, 4263–4271,
915 10.1016/j.atmosenv.2011.04.082, 2011.

916